4

Patterns and Organisation in Precipitation

Efi Foufoula-Georgiou and Venugopal Vuruputur

4.1 INTRODUCTION

Rainfall possesses a complex spatio-temporal structure which has been the subject of many studies. Traditionally, applied hydrologists have recognised the importance of this structure on runoff production, and have tried to analyse and model it using simple descriptions, such as the depth–area–duration (DAD) curves, the area-reduction curves, and the hyetographs or normalised hyetographs (see Chow et al., 1988; Linsley et al., 1982; Viessman and Lewis, 1996). The DAD curves depict, for a given duration, the area of the storm over which a given depth is equalled or exceeded. The area-reduction curves depict, for a given duration again, the decrease of the maximum storm depth (measured at a point) when it is averaged over increasing areal extent around that point. The normalised hyetograph (or mass curve) depicts, at a particular location or as average over an areal extent, the percentage of total storm depth (normalised depth) versus the percentage of storm duration (normalised time).

The above are of course simple measures of the complex spatio-temporal variability of the observed storm patterns, but still provide a means of comparing observed patterns to each other or to extremes. They also provide the means of parameterising design storms and reconstructing their spatio-temporal patterns to be used in predicting design hydrographs through rainfall-runoff modelling. For example, a 12-hour design storm depth at a point (computed from a frequency analysis or from the Probable Maximum Precipitation methodology) can be converted to "a design storm pattern" by assigning it a DAD curve and a design mass curve. That is, the spatial internal structure of the design storm could be reconstructed using the selected design DAD curves and an assumed shape for isohyets, and the temporal distribution of the total rainfall depth over its duration could be obtained using the selected design mass curve. All these attempts to reconstruct the space-time variability of a storm were based on the recognition that this variability plays an important role in runoff production (e.g., see Kiefer

Rodger Grayson and Günter Blöschl, eds. *Spatial Patterns in Catchment Hydrology: Observations and Modelling*

and Chu, 1957; Huff, 1967; Pilgrim and Cordery, 1975; and Milly and Eagleson, 1988; among others). It should be noted that in the early hydrology days, due to data limitations (typically one or a few raingauges over the basin) more detailed descriptions of the storm spatiotemporal patterns were not possible.

The recognition of the importance of the small-scale space-time rainfall variability on runoff modelling led to considerable research efforts in developing stochastic point process models or phenomenological spatiotemporal models of rainfall which could be used to simulate precipitation patterns, conditional on preserving a desired total depth (e.g., see Gupta and Waymire, 1979; Kavvas and Delleur, 1981; Waymire et al., 1984; Valdes et al., 1985; Seed et al., 1999; see also the review of Foufoula-Georgiou and Georgakakos, 1991). In more recent years, the wide availability (at least in the United States) of NEXRAD or other radars that continually monitor rainfall at high spatial and temporal resolution (typically pixels of 2 or 4 km and at intervals of 6–10 min) have provided unique opportunities to better understand and quantify the small-scale rainfall variability. These efforts have provided considerable insight on the effect of rainfall resolution on the accuracy of runoff production estimates (e.g., see Kouwen and Garland, 1989; Krajewski et al., 1991; Ogden and Julien, 1993, 1994; Michaud and Sorooshian, 1994a; Obled et al., 1994; Faurès et al., 1995; and Winchell et al., 1998) despite the still unresolved problems related to the accuracy of the NEXRAD estimates of precipitation (e.g., see Collier and Knowles, 1986; Pessoa et al., 1993; among others). Also, the need to unify descriptions over scales (i.e., rainfall variability over a small area with rainfall variability over a larger scale) and to parameterise subgrid-scale rainfall variability parsimoniously, has prompted the introduction of new ideas and tools for analysing and modelling space-time rainfall patterns, namely, the ideas of scale-invariance (see Schertzer and Lovejoy, 1987; Gupta and Waymire, 1990; Kumar and Foufoula-Georgiou, 1993a,b; among others).

Scale invariance implies that variability of rainfall, or another quantity such as rainfall fluctuations, exhibits a statistically similar structure under proper renormalisation of space and/or time coordinates. The scale-invariance concept for rainfall has been conceptually justified based on the idea that, after all, raindrops are tracers in the turbulent atmosphere and thus the documented presence of scale-invariance in fully-developed turbulence might also be manifested in the rainfall fields produced. Irrespective of the theoretical rationale and foundation of the scale-invariance ideas of rainfall, compelling evidence has been accumulated over the past decade that indeed some features of rainfall exhibit scale invariance (for example, see Foufoula-Georgiou and Krajewski, 1995; and Foufoula-Georgiou and Tsonis, 1996). This evidence has paved the way for the development of new classes of space-time rainfall models which are applicable over a large range of scales. Models based on scale invariance are considerably more attractive compared to the previous generation of stochastic point process phenomenological models in that they: (a) are much more parsimonious, i.e., 2 or 3 parameters versus 10 to 12 parameters in the previous models; and (b) are

scale-independent, i.e., applicable to a wide range of scales without changes in the model parameterisation or parameter values.

Another approach to the generation of high-resolution space-time patterns of precipitation is via numerical weather prediction models. These models have been considerably advanced in recent years in terms of physical parameterisations, data assimilation and numerical schemes, but still require extensive computational resources to run at high resolutions (e.g., see Droegemeier, 1997). Typically, they run in a nested mode where higher resolution domains are nested within a larger lower resolution domain which provides boundary fluxes and larger-scale environmental forcings to the smaller domain. The very high resolution domain involves sophisticated microphysics suitable to explicitly resolve cumulus-scale convection. The outer domain typically uses convective parameterisation schemes which depend on the model resolution. The accuracy of quantitative precipitation forecasts (QPFs) produced by these models has not been fully evaluated yet and is an issue of ongoing research (e.g., see Fritsch et al., 1998). Moreover, several studies have demonstrated the sensitivity of the resulting precipitation patterns to the chosen convective parameterisation schemes (even if these schemes are only used at the lower-resolution outside domain), to the chosen model resolution, to the degree of prescribed heterogeneities, and to the land–atmosphere exchange mechanisms embedded in the model (e.g., see Kain and Fritsch, 1992; Sivapalan and Woods, 1995; Avissar and Liu, 1996; Brubaker and Entekhabi, 1996; Wang and Seaman, 1997; Warner and Hsu, 2000; among others).

This chapter concentrates on stochastic descriptions of space-time rainfall variability based on scale-invariant parameterisations. It reviews some of the recent research describing and modelling spatiotemporal rainfall patterns and demonstrates that indeed the seemingly complex patterns of rainfall exhibit simple underlying statistical structures which can be unravelled with proper methodologies. We focus only on spatiotemporal descriptions based on scaling of rainfall fluctuations. Other descriptions based on multiscaling of rainfall intensities or multiplicative cascades (e.g., Schertzer and Lovejoy, 1987; Tessier et al., 1993; Over and Gupta, 1994; Seed et al., 1999) are not reviewed herein and the reader is referred to the original publications for such developments or to Foufoula-Georgiou and Krajewski (1995) for a brief review and further references.

Our presentation in this chapter evolves around three major questions:

1. If spatio-temporal patterns of rainfall exhibit an organised structure, how can this be used in building parsimonious models which are applicable over a range of scales and can also be used for the purpose of downscaling (i.e., reconstructing small-scale variability from large-scale averages)? This last issue is especially important given the increasing availability of remotely-sensed data whose reliability is often considered adequate only if observations are averaged over large scales, and also given the need to interpret the results of global or continental scale studies to the hydrologic basin scale.

2. If rainfall spatiotemporal patterns exhibit organisation, how can this help us to understand the still open question of relating the physics of the atmosphere with the statistics of the produced precipitation patterns?
3. If documentable space-time organisation exists in observed precipitation patterns, is the same structure reproduced by state-of-the-art numerical weather prediction models which eventually will be used to predict future storms and the resulting floods? And, moreover, what does the success or lack of success of the model in reproducing this structure tell us about the physics and parameterisations we currently use in atmospheric models?

4.2 SPATIAL RAINFALL ORGANISATION

To explain the idea of multiscale rainfall variability, consider the left-most field of Figure 4.1. It represents the radar-depicted rainfall intensity field of an extreme squall line storm of June 27, 1985 over Kansas and Oklahoma at 0300 UTC at a resolution of 4 km. If this field is degraded to different scales e.g., 8, 16, 32, 64 km by averaging, then the question arises as to whether the spatial rainfall variability of this field changes with scale in a systematic way. Moreover, notice that when we average or filter the process at a small scale to go to a larger scale, some "information" about its spatial variability is lost. This lost "information" when going from one scale to a coarser one by averaging can be preserved by keeping the so-called rainfall "fluctuations" (i.e. the difference in intensities in adjacent pixels in terms of space and/or time). If the variability of the rainfall intensities themselves does not exhibit a simple statistical structure over scales, could it be that such a structure exists in the rainfall fluctuations?

Kumar and Foufoula-Georgiou (1993a,b) and later Perica and Foufoula-Georgiou (1996a) performed a multiscale analysis of spatial rainfall fields using a discrete orthogonal wavelet transform. This transform within the multiresolution framework of Mallat (1989) provides a filter which simultaneously keeps the "averages" (smoothed fields) and "fluctuations" (details lost) as the scale changes. The two-dimensional orthogonal wavelet transform is a directional filter, so it can handle anisotropy, and is a reconstructive filter so that from the average field at 64 km and the fluctuations at scales 8, 16, 32 and 64 km, the field at the smaller scale (higher resolution) of 4 km can be reconstructed. Of course, statistical parameterisation of the details will result in a statistical reconstruction of the high-resolution field. These ideas give rise to three important questions: (a) does the spatial variability of the rainfall intensity fields at a range of scales, exhibit a simple structure which can be parameterised with a few coefficients?; (b) what about the structure of rainfall fluctuations or details as a function of scale?; and (c) what physical parameters might control the way this variability changes over scales?

These three questions were considered by Perica and Foufoula-Georgiou (1996a,b) who analysed a large number of mid-latitude mesoscale convective

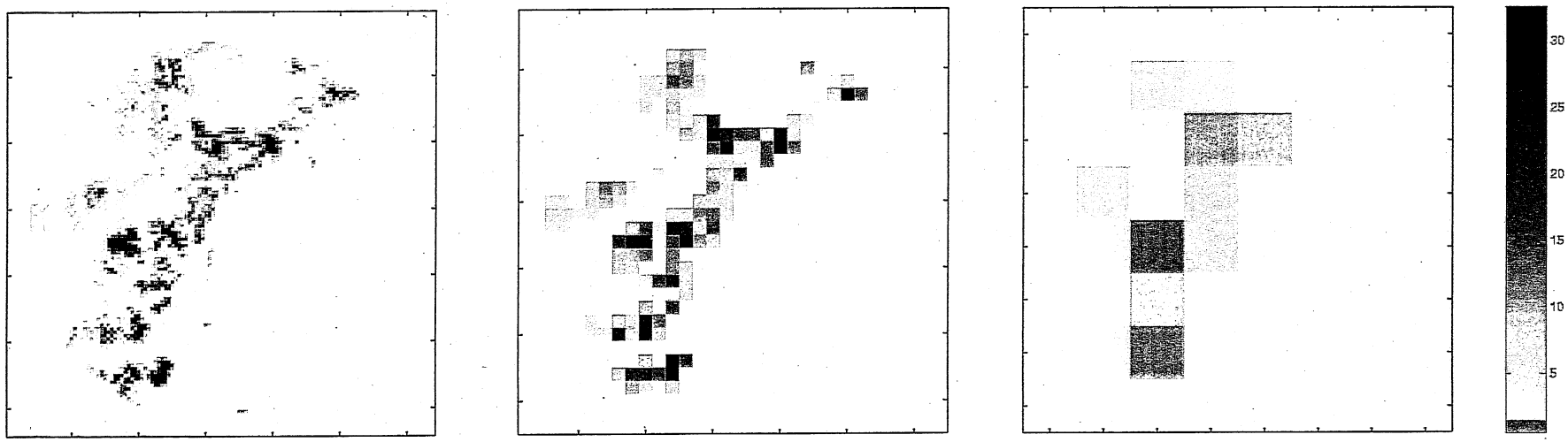

Figure 4.1. The June 27, 1985 storm over Kansas–Oklahoma at 0300 UTC. The left panel shows the observed radar fields at 4 km resolution and the middle and right panels show the degraded fields at 16 and 64 km resolution, respectively. The intensities have been mapped onto the same 32 colours for display purposes.

systems monitored by the Oklahoma–Kansas radar during the May–June, 1985 period of the Preliminary Regional Experiment for Storm-Central (PRESTORM) field program (see Cunning, 1986 for details of this experiment). It was found that although rainfall intensities themselves did not have a simple well-structured way of changing their variance as a function of scale, the "standardised rainfall fluctuations" i.e., rainfall fluctuations normalised by their corresponding-scale local rainfall averages, exhibited Normality and simple scaling, i.e., their variance changed with scale in a log–log linear way. This is not surprising since the multiscale rainfall averages carry in them the signature of deterministic background features which are particular to the rainfall-producing mechanism, making it unlikely for them to exhibit simple scaling relationships over a significant range of scales. However, once these underlying deterministic features are removed by filtering, the remaining features (e.g., deviations from local means or spatial rainfall gradients) do not seem to have a characteristic length scale and are more amenable to stochastic parameterisations which might present similarities over scales.

Specifically, let $\overline{X_\lambda}$ denote the value of the rainfall average at scale λ at a particular pixel, and $X'_{\lambda,i}$, the value of the rainfall fluctuation (difference of values at adjacent pixels) at the same scale λ and direction i (e.g., latitude, longitude and diagonal). Standardised rainfall fluctuations at scale λ and direction i are defined as $\xi_{i,\lambda} = X'_{\lambda,i}\sqrt{\overline{X}_\lambda}$. Perica and Foufoula-Georgiou (1996a) computed these standardised fluctuations using an orthogonal Haar wavelet transform and found that between scales of 4 km and 64 km, for which data were available, $\xi_{i,\lambda}$ exhibited Gaussianity and simple scaling implying that

$$\frac{\sigma_{\xi,L_1}}{\sigma_{\xi,L_2}} = \left(\frac{L_1}{L_2}\right)^H \tag{4.1}$$

where $\sigma_{\xi,L}$ is the standard deviation of ξ at scale L km and H is a scale-independent parameter. The values of H varied between 0.2 and 0.5 for several mid-latitude mesoscale convective systems from the PRESTORM data set. The dependence of H on direction was not very pronounced but H was found to be strongly dependent on the convective instability of the prestorm environment, as measured by the convective available potential energy, CAPE (in m^2s^{-2})

$$H = 0.0516 + 0.9646 \cdot (\text{CAPE} \times 10^{-4}) \tag{4.2}$$

(see Figure 4.2). CAPE is the buoyant energy available to a parcel rising vertically through an undisturbed environment and is a measure of the potential instability at middle to upper atmosphere. It is defined as

$$\text{CAPE} = \int_{\text{LFC}}^{\text{EL}} g \cdot \left(\frac{\Theta_c - \Theta_{\text{env}}}{\Theta_{\text{env}}}\right) dz \tag{4.3}$$

where Θ_c is the potential temperature of an air parcel lifted from the surface to level z, Θ_{env} is the potential temperature of the unsaturated environment at the

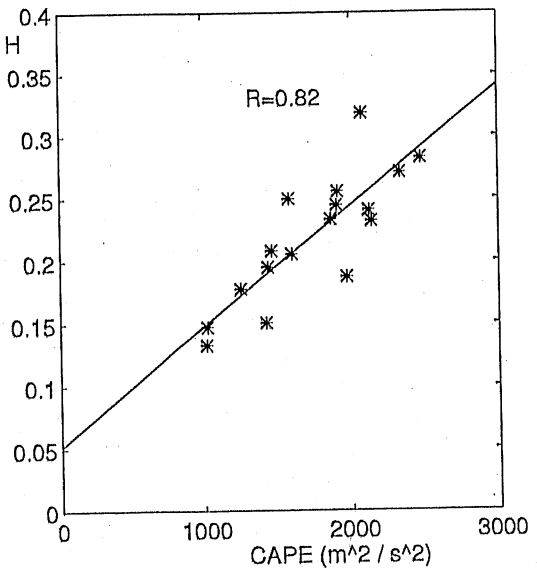

Figure 4.2. Scattergram indicating the relationship between the scaling parameter H of the standardised rainfall fluctuations and the Convective Available Potential Energy (CAPE) in m^2/s^2 of their prestorm environment. Data were used from several midlatitude mesoscale convective systems of the PRESTORM field program (after Perica and Foufoula-Georgiou, 1996a).

same level, LFC is the level of free convection and EL is the equilibrium level (e.g., see Air Weather Service, 1979; General Meteorological Package (GEMPAK), 1992).

The empirical relationship between H and CAPE is useful since CAPE can be computed from observed sounding data or by a numerical weather prediction model and then H can be estimated from (4.2) and used to infer the variability of rainfall fluctuations at any scale, given the variability at a reference scale (see also Perica and Foufoula-Georgiou, 1996b). For more information on the linkage of CAPE, and some other meteorological parameters, to statistical parameterisations of rainfall fluctuations, the reader is referred to Perica and Foufoula-Georgiou (1996a). Application examples are given in Section 4.4.1.

4.3 SPATIOTEMPORAL DYNAMICS

Spatial and temporal features of rainfall are not independent of each other but relate in ways specific to the physics of the storm-generating mechanisms. Thus, a lot of insight may be gained by studying simultaneously the spatial and temporal patterns of rainfall. Recently, Venugopal et al. (1999a) developed a methodology under which space and time structures of rainfall can be studied simultaneously at a multitude of scales. Using this methodology, they demonstrated that there exists a simple scale-invariant spatiotemporal organisation in rainfall patterns which can be unravelled by proper renormalisation of the space and time coordinates.

Let $I^L_{i,j}(\tau)$ and $I^L_{i,j}(\tau + t)$ represent rainfall intensity values averaged over a box of size L centered around spatial location (i, j) of the precipitation field at two instants of time τ and $\tau + t$, respectively (Figure 4.3). The evolution of the field at scale L and a time period t was characterised in Venugopal et al. (1999a) by the differences in the logs of the rainfall intensities $\Delta \ln I$, i.e.,

$$\Delta \ln I_{i,j,\tau}(L, t) = \ln\left(I^L_{i,j}(\tau + t)\right) - \ln\left(I^L_{i,j}(\tau)\right) \tag{4.4}$$

computed at all spatial locations (i,j). This selection (as opposed to the simpler selection of intensity differences, i.e., $\left[I^L_{i,j}(\tau + t) - I^L_{i,j}(\tau)\right]$) was made since there is evidence that the rainfall process is not additive but rather multiplicative, that is, normalised rainfall fluctuations, $\Delta I/I \equiv (I - I')/(I + I')/2$ in the terminology of Figure 4.3, and not fluctuations ΔI themselves, are independent random variables and spatially uncorrelated (see Venugopal et al., 1999a). This implies that fluctuations of ln(rainfall), i.e., $\Delta \ln I = \ln I - \ln I'$ are independent and also spatially uncorrelated random variables and can be easily characterised statistically.

The measure described above was evaluated for all locations (i,j) and all time instants τ, and for various spatial and temporal scales, L and t, respectively. Then assuming stationarity in space (i.e., independence of the specific (i,j) position) and selecting stationary regions in time (i.e., regions where the statistics of $\Delta \ln I$ do not fluctuate significantly around their mean value for the region), the probability density functions (PDFs) of $\Delta \ln I(L, t)$ were used to characterise the evolution of rainfall at several spatial scales L and temporal scales t. Notice that homogeneity in space is a reasonable assumption given that the radar frame can be seen as a fixed window within which the moving storm is observed. Thus, unless there is a specific reason to believe that a portion of the radar frame receives statistically different rainfall than the rest of the frame, intensities (or $\Delta \ln I$'s) at all positions (i,j) are considered to come from the same probability distribution.

Venugopal et al. (1999a) and Venugopal (1999) found, by analysis of several storms in different geographical regions of the world (the tropical region in Darwin, Australia; the forested region of Northern Saskatchewan, Canada; and the Oklahoma region in the midwestern United States), that the PDFs of $\Delta \ln I(L, t)$ remain statistically invariant if space and time are renormalised with the transformation $t/L^z = constant$. That is, the evolution of the rainfall field at scale L_1 and during a time lag t_1 is statistically identical to the evolution of the rainfall field at spatial scale L_2 and time lag t_2, as long as

$$t_1/t_2 = (L_1/L_2)^z \tag{4.5}$$

where z is the socalled dynamic scaling exponent.

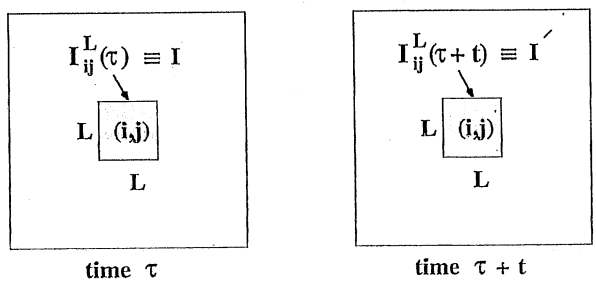

Figure 4.3. Schematic illustrating the change in intensity of a field (rainfall in this case) over a box of size $L \times L$ centred around the location (i,j) during a time interval t.

Table 4.1. Standard deviations of $\Delta \ln I$ ($\Sigma(\Delta \ln I)$) with time lag (left to right) and aggregation level (top to bottom), for a stationary region of the storm of Dec. 28, 1993, in Darwin, Australia

		Time Lag t (min)							
		10	20	30	40	50	60	70	80
L (km)	2	0.58	0.77	0.89	0.97	1.05	1.11	1.17	1.21
	4	0.47	0.67	0.79	0.87	0.95	1.01	1.07	1.12
	8	0.35	0.55	0.67	0.76	0.84	0.90	0.96	1.01
	16	0.23	0.40	0.53	0.63	0.71	0.77	0.83	0.88

Table 4.1 shows the matrix of standard deviations of these PDFs of $\Delta \ln I(L, t)$ for different spatial scales, L, and temporal scales, t, for a stationary portion of duration five hours of the December 28, 1993 storm in Darwin, Australia (see Venugopal et al., 1999a for a description of this storm). Notice that these PDFs are well approximated by normal distributions centred around zero at all space and time scales (see Figure 4.4) and thus their standard deviation completely parameterises them.

From Table 4.1, one can find, by interpolation, pairs of (L, t) such that a chosen value of the standard deviation $\Sigma(\Delta \ln I)$ remains constant. For example, Table 4.2 displays pairs (L, t) for which $\Sigma(\Delta \ln I)$ remains constant and equal to 0.6, 0.7 and 0.8, respectively. If these pairs satisfy $t \sim L^z$ i.e., if the iso-standard deviation lines plot linear on a log–log plot of L versus t, then the process is said to exhibit dynamic scaling. Figure 4.5 (left panel) shows the log–log plot of the values of Table 4.2. The fitted lines are for $\Sigma(\Delta \ln I) = 0.8$, 0.7 and 0.6 (top to bottom) and give estimates of z equal to 0.51, 0.54 and 0.58, respectively. Obviously, these iso-standard deviation lines are well approximated by straight lines implying that rainfall evolution (as characterised by the PDF of $\Delta \ln I$) exhibits dynamic scaling. Note that since the PDF of $\Delta \ln I(L, t)$ is well approximated by a Normal distribution, scale-invariance of $\Sigma(\Delta \ln I)$ implies scale invariance in the whole PDF. This was verified by computing (via interpolation) the PDFs of $\Delta \ln I$ at several (L, t) pairs which satisfy $t \sim L^z$ (for example, the pairs in Table 4.2) and checking that indeed these PDFs remained statistically invar-

Table 4.2. Time (in min) to "reach" different values of the standard deviation of $\Delta \ln I$ (left to right: 0.6, 0.7, 0.8) for various aggregation levels (top to bottom), for a stationary region of the storm of Dec. 28, 1993, in Darwin, Australia. This table is formed by linear interpolation of the values in Table 4.1

		$\Sigma(\Delta \ln I)$		
		0.6	0.7	0.8
L (km)	2	11.1	16.3	22.4
	4	16.6	22.8	31.6
	8	24.4	33.3	45.1
	16	37.4	49.4	64.7

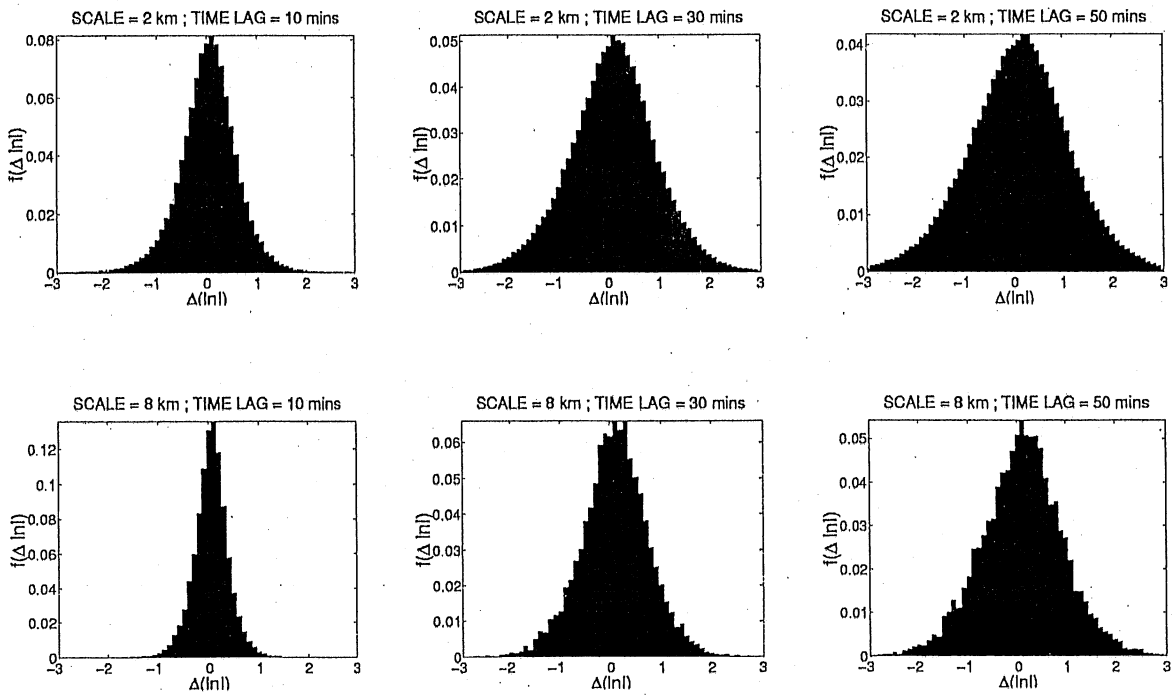

Figure 4.4. Selected PDFs of $\Delta \ln I$ (top: spatial scale of 2 km and time lags of 10, 30 and 50 min; bottom: spatial scale of 8 km, and time lags of 10, 30 and 50 min) for a stationary region of the storm of Dec. 28, 1993, in Darwin, Australia.

iant (see Figure 4.6). Similar results were found for several other storms in Darwin, Australia (see Figure 4.5 for the storm of January 4, 1994), the BOREAS region in northern Saskatchewan, and the midwestern United States region (see Venugopal, 1999).

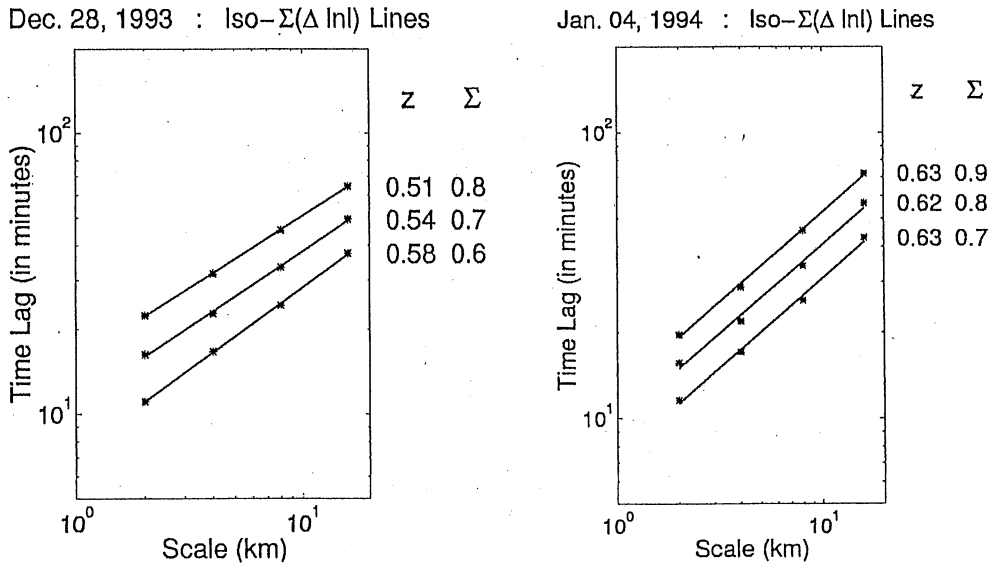

Figure 4.5. Plot illustrating the presence of dynamic scaling in the standard deviations of $\Delta \ln I$ for (a) a stationary region of the storm of Dec. 28, 1993 (left) and (b) a stationary region of the storm of Jan. 4, 1994 (right) in Darwin, Australia.

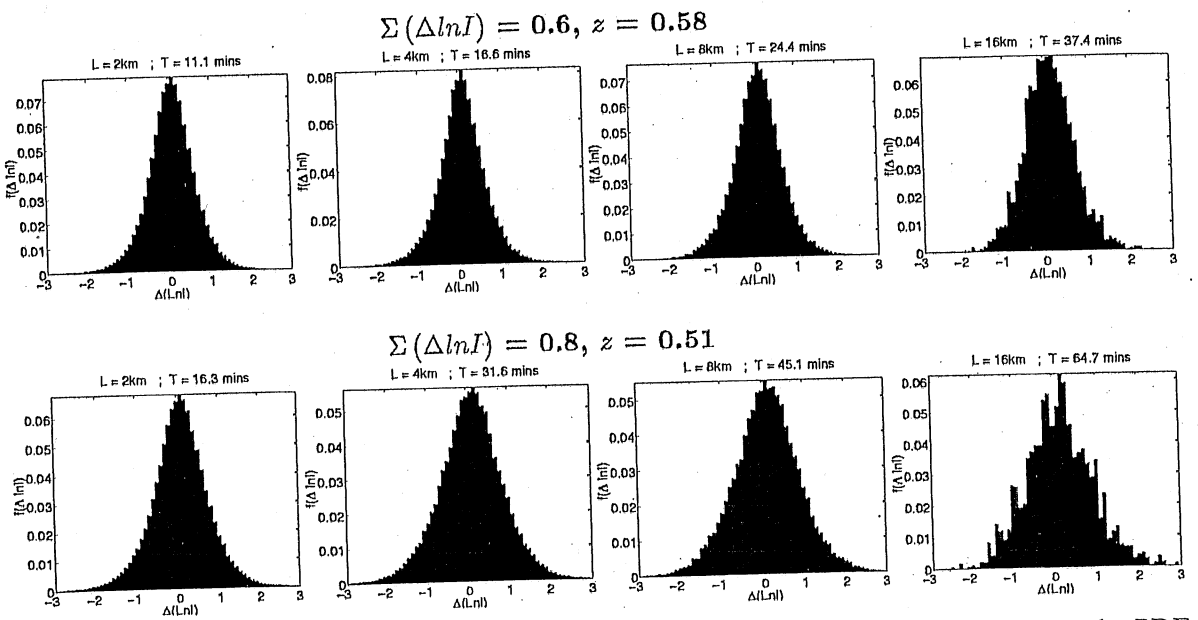

Figure 4.6. For a stationary region of the storm of Dec. 28, 1993: Confirmation that the PDFs remain statistically invariant under the transformation $t/L^z = \text{constant}$. The top row shows PDFs for $\Sigma(\Delta \ln I) = 0.6$, $z = 0.58$ and pairs of (t, L) which satisfy $t/L^z = \text{constant}$ (see Table 4.2). The bottom row shows the same for $\Sigma(\Delta \ln I) = 0.8$, $z = 0.51$. Similar result holds for $\Sigma(\Delta \ln I) = 0.7$, $z = 0.54$.

The above results imply that, given the statistical structure of rainfall evolution at large scales, the structure at small scales can be statistically predicted. Application examples are given in Section 4.4.2.

4.4 RAINFALL DOWNSCALING FOR HYDROLOGIC APPLICATIONS

4.4.1 Spatial Downscaling

Recall from Section 4.2, that knowing the spatial variability of rainfall fluctuations at several intermediate scales permits the statistical reconstruction of the rainfall intensities themselves from a larger scale to a smaller scale, e.g., from 64 km down to 4 km. Based on the scale invariance of standardised rainfall fluctuations (equation (4.1)) and the relation of the scaling parameter H to CAPE (equation (4.2)), a spatial rainfall downscaling scheme was developed and implemented to several mid-latitude mesoscale convective systems with considerable success (Perica and Foufoula-Georgiou, 1996b). This scheme is able to statistically reconstruct the small-scale spatial rainfall variability and the fraction of area covered by the storm, given the large-scale rainfall field and value of CAPE in the prestorm environment i.e., ahead of the storm (see Zhang and Foufoula-Georgiou, 1997 for a numerical study of the spatial variability of CAPE and definition of a representative value of CAPE for use in (4.2)).

This spatial downscaling scheme has the advantage that its parameterisation is scale-independent and thus offers the capability of resolving the subgrid-scale spatial rainfall variability at any desired scale (at least between 4 km and 64 km,

that the relationships were developed) without the need to consider a separate parameterisation scheme at each scale. Figure 4.7 shows an example where the downscaling scheme was used to disaggregate rainfall from the scale of 64 km to the scale of 4 km. It is seen that the disaggregated field compares well to the actual field. More details and a formal statistical comparison of these fields can be found in Perica and Foufoula-Georgiou (1996b) and application to other mesoscale complexes in Perica (1995). It is noted that recent evidence by Zhang and Foufoula-Georgiou (unpublished manuscript) using multi-radar data of the COMET project, suggests that the predictive relationships between H and CAPE may hold up to scales of 256 km.

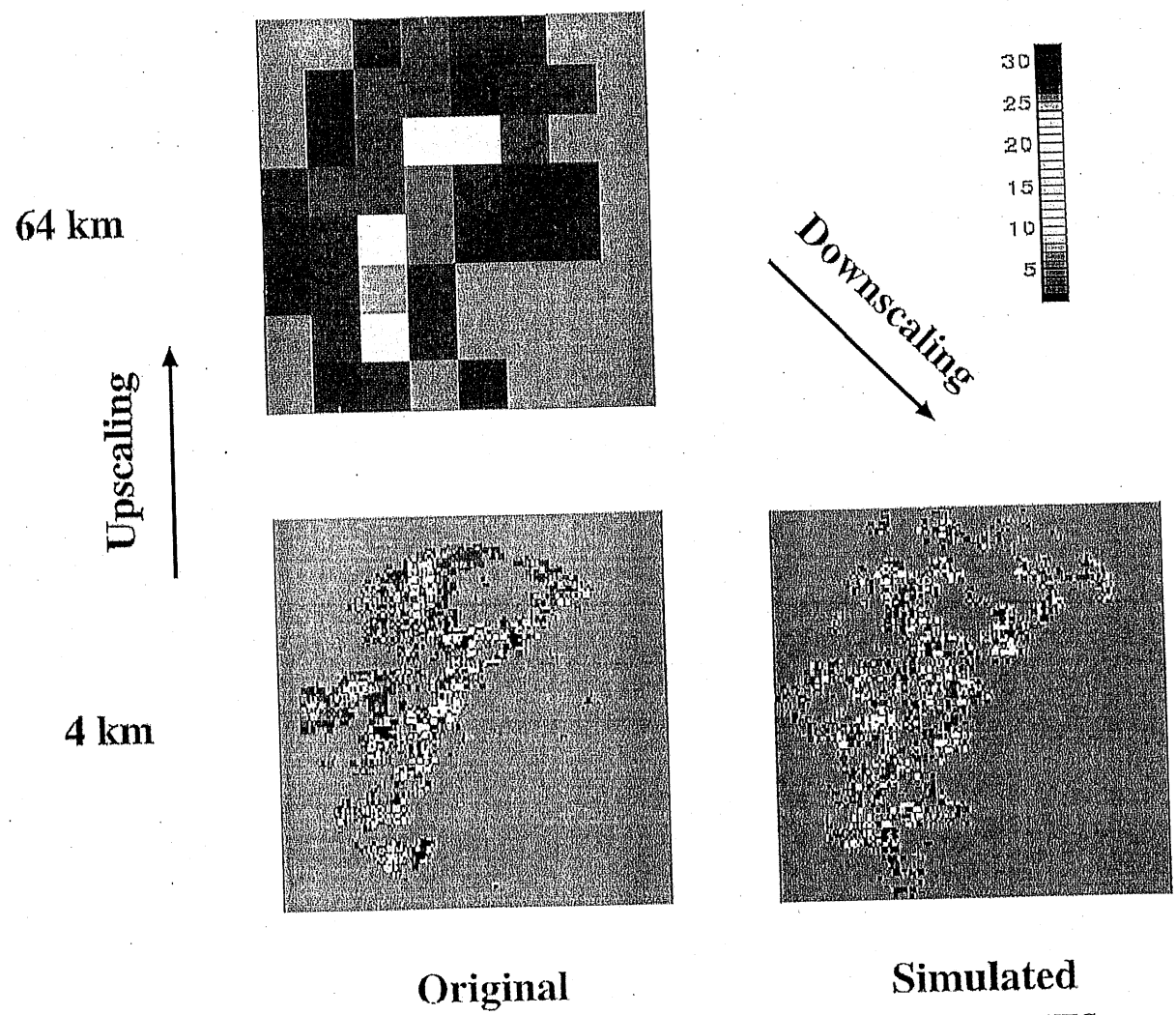

Figure 4.7. Spatial downscaling of the June 27, 1995 storm over Kansas–Oklahoma at 0300 UTC from 64 km to 4 km scale. A good agreement is found between the downscaled field (bottom right panel) and the observed field at the same resolution (bottom left panel). The intensities have been mapped onto the same 32 colours for display purposes.

4.4.2 Spatiotemporal Downscaling

Note that in the above spatial downscaling scheme, the spatial correlation of the small-scale rainfall is well preserved (see Perica and Foufoula-Georgiou, 1996b). However, if the scheme is applied independently at different instants of time, there is no guarantee that the temporal correlation (persistence) at the subgrid scales will also be preserved. In fact, a wet pixel at one instant might become dry at the next, still preserving the statistical spatial structure of the field. This might be a problem if the downscaled values were to be used in a continuous rainfall/runoff model where the "memory" of the system (e.g., soil moisture accumulation) must be well captured for accurate runoff prediction.

Recently, Venugopal et al. (1999b) proposed a new downscaling scheme which explicitly attempts the statistical preservation of both the spatial and temporal correlation of rainfall at the subgrid scales. This scheme takes advantage of the presence of dynamic scaling in rainfall evolution discussed in Section 4.3. There are several technicalities in the implementation of the spatio-temporal downscaling scheme, but the essence remains the following: small-scale space-time structures relate to larger-scale ones (in fact the PDFs of $\Delta \ln I$ remain statistically invariant) if an appropriate transformation of space and time, namely, $t \sim L^z$, is applied. Thus, given the statistical structure of rainfall at large scale, the small-scale space-time features can be statistically reconstructed based on dynamic scaling. This model is schematically depicted in Figure 4.8 and extensively discussed in Venugopal et al. (1999b).

Figure 4.9 shows the results of applying this space-time downscaling scheme to the storm of January 4, 1994 in Darwin, Australia. We started with the large-

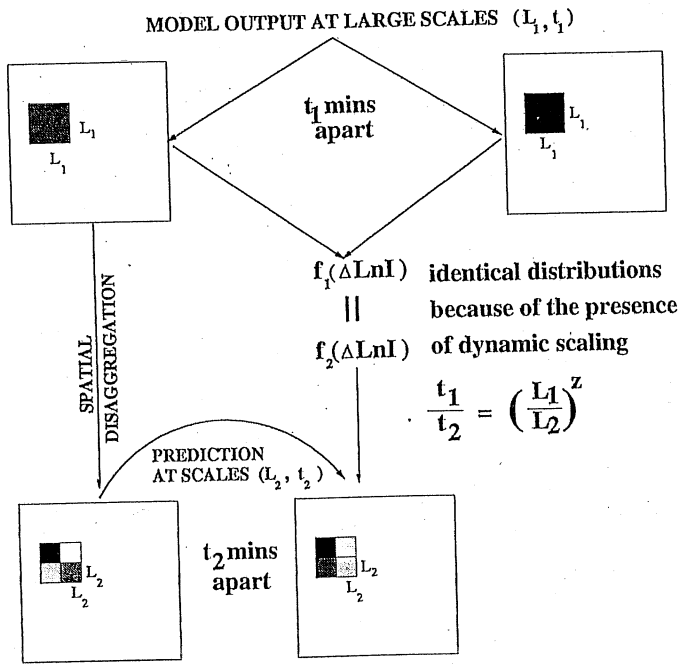

Figure 4.8. Schematic of the space-time downscaling scheme of Venugopal et al. (1999b) illustrating how the framework of dynamic scaling is coupled with an existing spatial disaggregation scheme to predict rainfall evolution at smaller space-time scales.

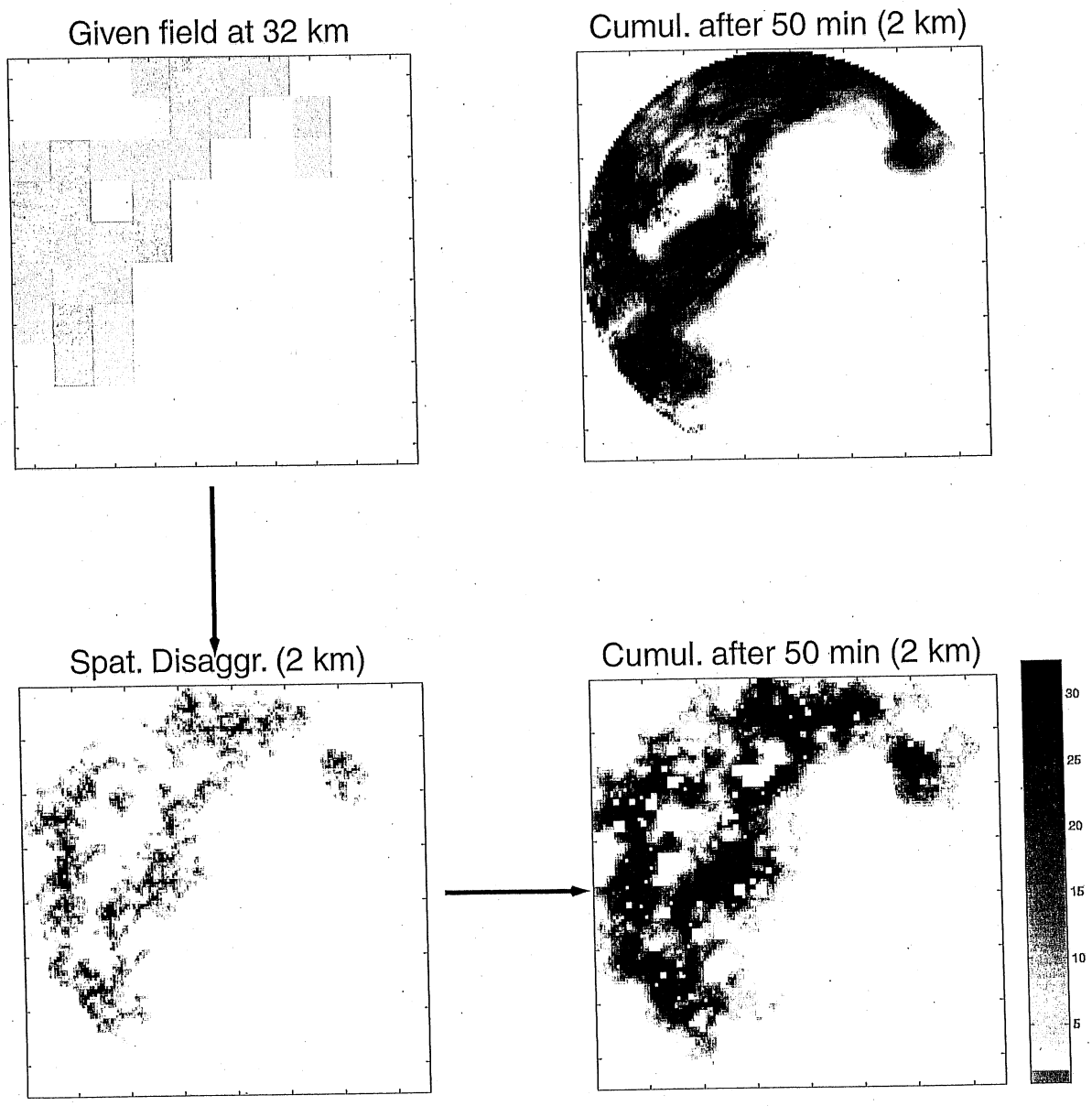

Figure 4.9. Storm of Jan. 4, 1994, in Darwin, Australia: Validation of the proposed space-time downscaling scheme by comparing the predicted 50-min cumulative rainfall patterns (bottom right panel) to the observed ones (top right panel).

scale field at 32 km (top left panel) at an instant of time (1831 UTC). This field was spatially downscaled to 2 km (see bottom left panel) using $H = 0.4$ in the scheme of Perica and Foufoula-Georgiou (1996b) discussed in the previous section. Then, the space-time scheme of Venugopal et al. (1999b) was used to evolve the 2 km field over time. It was assumed that large-scale (32 km) fields were available to us every 10 minutes. These data were used to update the distribution of changes at the large scale (32 km) which is identical to the distribution of changes at the small scale (2 km) according to the dynamic scaling hypothesis we put forth in Section 4.3.

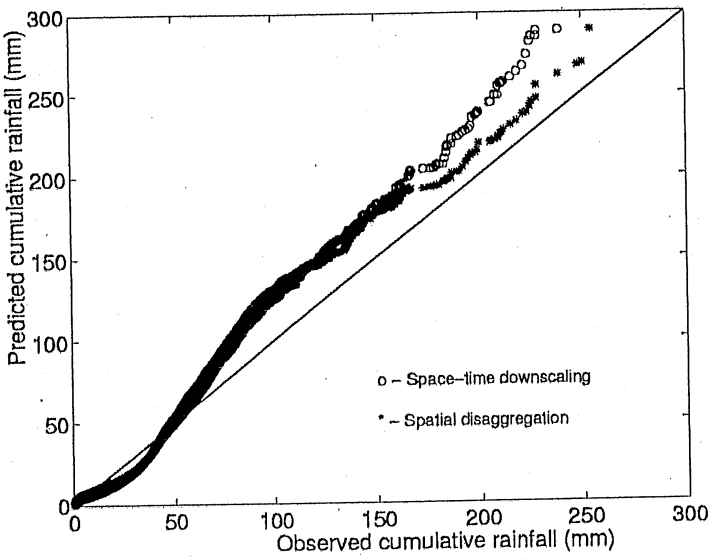

Figure 4.10. Storm of Jan. 4, 1994 in Darwin, Australia: Comparison of the observed 50-min cumulative rainfall amounts (in mm) to those predicted by space-time downscaling (circles) and spatial downscaling only (asterisks).

Figure 4.9 (bottom right panel) shows the 50-minute cumulative rainfall fields at a scale of 2 km predicted from the space-time downscaling scheme. In the same figure, the observed 50 minute cumulative field is also shown for comparison (top right panel). Visually, the space-time downscaled field compares well with the observed field (see Venugopal et al., 1999b for an extensive quantitative comparison). It is noted that, although for this storm the space-time downscaling scheme seems to overestimate the extreme 50-minute accumulations slightly more than the spatial downscaling scheme applied independently in time (see Figure 4.10), the space-time scheme is able to reproduce the temporal correlation at the subgrid scales much better than the spatial scheme alone (see Figure 4.11).

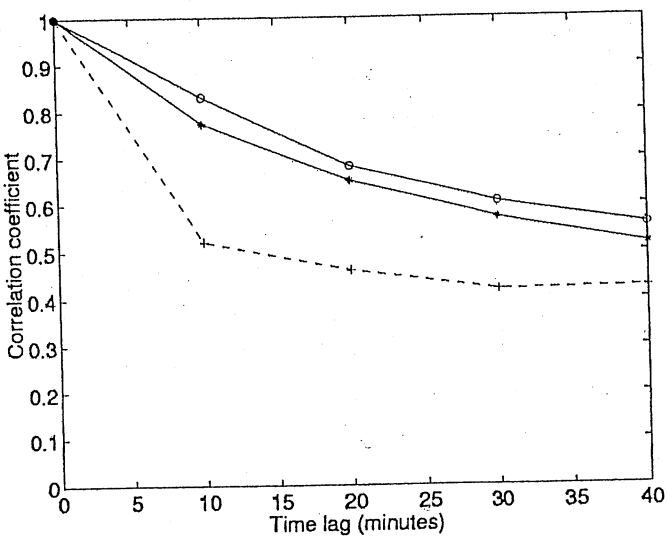

Figure 4.11. Storm of Jan. 4, 1994, in Darwin, Australia: Comparison of the temporal correlation at the 2-km scale computed from the observed fields (asterisks), from the predicted fields by the space-time downscaling scheme (circles) and by the spatial downscaling scheme only (dashed line).

Overall it is concluded that the space-time downscaling scheme discussed above is able to successfully reproduce the spatial and temporal correlation of rainfall at the subgrid scales given large-scale averages of precipitation and the downscaling parameters, H and z (see also Venugopal et al., 1999b for other applications and extensive quantitative evaluation of model performance). Providing downscaled 2 km precipitation fields in a rainfall-runoff model is expected to yield more accurate estimates of runoff and other fluxes as compared to those that would be obtained if the 32 km precipitation fields were used. Also, preserving temporal persistence in the downscaled rainfall is important in many hydrologic studies since the time-history of rainfall intensities is known to affect soil-moisture storage and runoff production from a basin. The exact degree to which the predicted runoff is affected by including or ignoring temporal persistence of rainfall at the subgrid scale remains yet to be quantified. Such a study is currently in progress in our group and the results will be reported in the near future.

4.5 CAN ATMOSPHERIC MODELS REPRODUCE THE OBSERVED PRECIPITATION PATTERNS?

Accurate forecasting of the onset, duration, location and intensity of precipitation via numerical weather prediction models, remains still a difficult challenge. Generally efforts in model development (in terms of physical and numerical advances) have outpaced efforts in detailed model validation. Specifically, methods that compare the forecasted high-resolution precipitation patterns to the observed ones, such that deficiencies in microphysical parameterisations and other small-scale structure representations can be depicted, lag behind. Traditional measures of forecast performance are too coarse for this purpose and provide only limited information about the ability of the numerical weather prediction model to mimic the dynamical environment of the storm which created the observed complex spatiotemporal rainfall pattern. Consequently, they also provide limited feedback as to how to go about improving the model (in terms of microphysical parameterisation, data assimilation, increased resolution, etc.) since they cannot quantitatively assess the detailed effect of these improvements on the forecasted precipitation pattern.

In a recent paper (Zepeda-Arce et al., 2000) several new multiscale statistical measures which can depict how well the small scale-to-scale variability and organisation of the forecasted fields matches that of the observed fields were proposed. It was demonstrated that indeed these measures are very informative compared to traditional measures of forecast verification and may lead to useful feedback for atmospheric model improvement. Some of these results are briefly discussed below.

In Zepeda-Arce et al. (2000), the multi-squall line of May 7–8, 1995 over Oklahoma was modelled by a state-of-the-art three-dimensional nonhydrostatic storm-scale prediction model (the Advanced Regional Prediction System – ARPS; see Droegemeier et al., 1996a,b; Xue et al., 1995; and Xue et al.,

2000a,b). The simulated rainfall patterns (available at the model resolution of 6 km) were compared to the observed ones (available at the radar resolution of 4 km) over a range of scales. Specifically, the predicted and observed fields were analysed for the presence of spatial and spatiotemporal scale invariances and the results compared.

The 18 minute rainfall accumulations from the observed radar patterns and 15 minute accumulations from the predicted patterns were analysed for scaling in spatial rainfall fluctuations. Good scaling was judged by a correlation coefficient of $R \geq 0.95$ in the log–log plots of the standard deviations of normalised spatial fluctuations with scale in the latitudinal and longitudinal directions and $R \geq 0.9$ in the diagonal direction (since there is greater uncertainty in estimating these values – see Perica and Foufoula-Georgiou, 1996b for their interpretation). Figure 4.12 shows the results of the analysis. When scaling was not present the estimated values of H are given, but the lack of scaling is marked on the plot by a dark square. As can be seen from Figure 4.12, the model was not able to reproduce the pronounced temporal variation of H_1, H_2, and H_3 during the storm evolution. Moreover, no directionality seemed to be present in the observed patterns ($H_1 \approx H_2 \approx H_3$) while the diagonal component (H_3) was significantly higher than H_1 and H_2 (by approximately 0.2) in the model. Generally, it was found that when scaling was present, $H_{\text{model}} < H_{\text{obs}}$. However, the standard deviations of the normalised fluctuations in all directions were higher in the model than in the observations, i.e., $\sigma_{\xi,\text{model}} > \sigma_{\xi,\text{obs}}$. These findings indicate that the model-predicted normalised rainfall fluctuations are in general more variable than the observed ones. However, the growth of this variability with scale is slower in the model than in the observations, at least for the longitudinal and latitudinal components. The drastic change in the values of H during the period of $t = 11$ to 13 hours (see Figure 4.12, top) was caused by the fact that at around $t = 11$ hours, a new squall-line started entering the domain of observation. This squall-line stayed in the domain until the end of the simulation period while the original squall-line moved out of the domain at around $t = 13$ hours. During the transition period ($t = 11$ to 13 hours) the statistical structure of the precipitation field within the domain of observation was different than before or after the transition. This, however, was not reproduced by the model-predicted patterns which had constant to only slightly increasing values of H during that period.

The radar-observed and model-predicted rainfall accumulations were also analysed for the presence of dynamic scaling within a stationary region of a few hours over which the mean and standard deviation of $\Delta \ln I$ did not vary significantly (see Zepeda-Arce et al., 2000 for details). For this region, the PDFs of $\Delta \ln I$ for spatial scales $L = 4$, 8, 16, and 32 km and temporal scales $t = 6$, 12, 18, 24, 30, 36, 42, 48, 54 and 60 min for the observed patterns were computed. For the predicted patterns the spatial scales were $L = 6$, 12, 24 and 48 km and temporal scales were $t = 15$, 30, 45, 60, 75 and 90 min. Then, the standard deviations of these PDFs were computed and (by interpolation in a tabular format) pairs of (L, t) were found which resulted in the same values of the standard deviation of $\Delta \ln I$ (see discussion in Section 4.3). This was done for

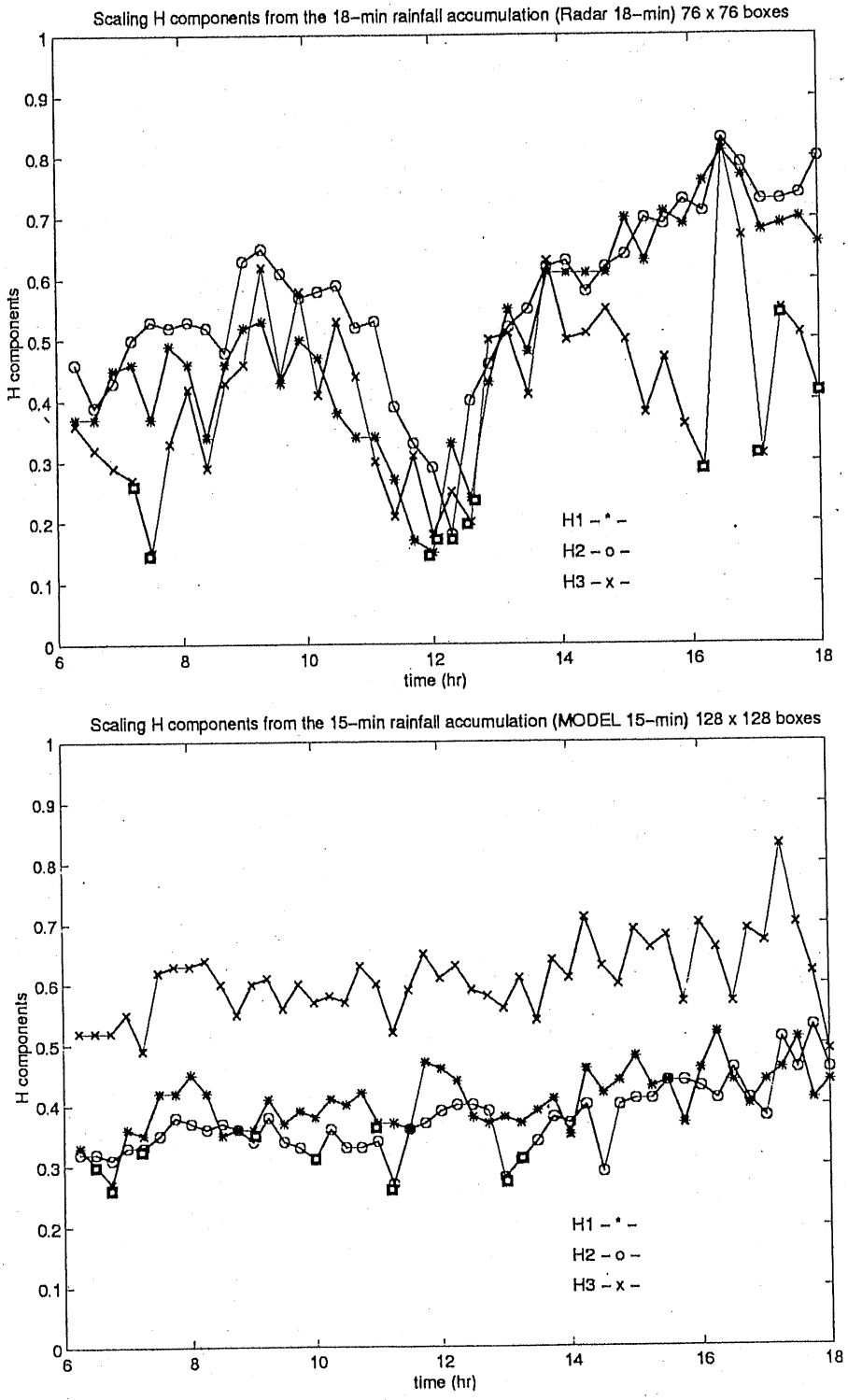

Figure 4.12. Scaling parameters H_1, H_2 and H_3 vs time from the 18-min observed (top) and 15-min simulated (bottom) rainfall accumulation patterns for the May 7–8, 1995 storm. Dark squares indicate the lack of scaling in normalised fluctuations.

both the observed and predicted patterns. These pairs (L, t) were plotted on a log–log plot as shown in Figure 4.13. It was observed that, to a good approximation, the (t, L) transformation under which the standard deviation of $\Delta \ln I$ remained constant was of the form $t/L^z = \text{constant}$ (i.e., straight-line relation-

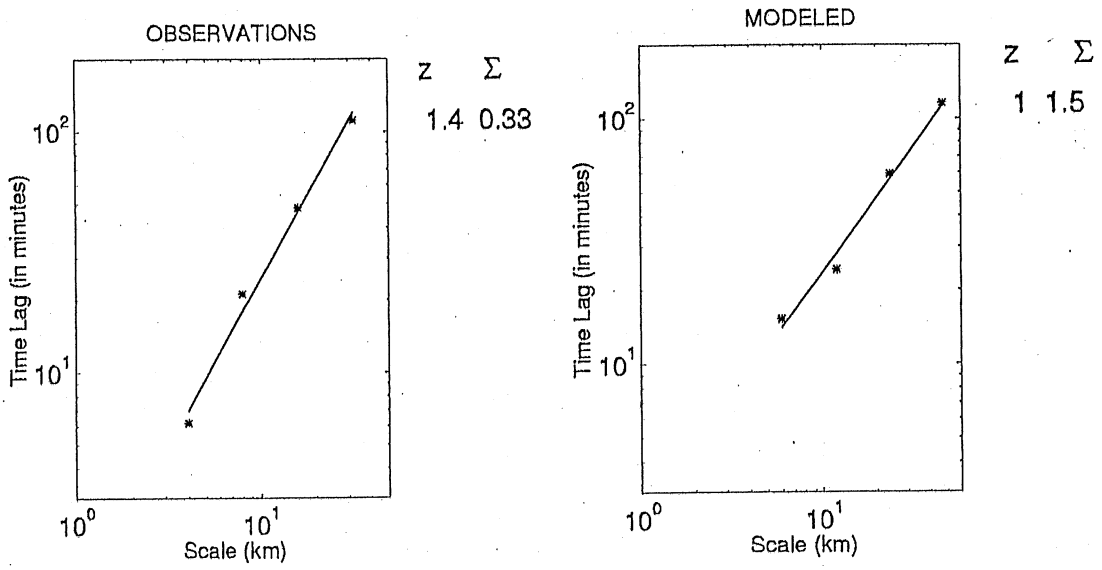

Figure 4.13. Dynamic scaling in the observed and predicted patterns of the May 7–8, 1995 storm over Oklahoma. For the observations, the iso-standard deviation line is for $\Sigma(\Delta \ln I) = 0.33$ and the estimate of $z = 1.4$; for the modelled field, $\Sigma(\Delta \ln I) = 1.5$ and $z = 1$.

ships on the log–log plots) for both the observed and predicted patterns. However, the values of z (estimated from the slopes of the log–log plots) were significantly different: $z = 1.4$ for the observed patterns and $z = 1.0$ for the predicted patterns. Also, the values of the standard deviations of $\Delta \ln I$ were much higher in the model than in observations. For example, in Figure 4.13, $\Sigma(\Delta \ln I)$ for the observations and the model-predicted fields was 0.33 and 1.5, respectively. This implies that for the same spatial scale and same time lag, the model-predicted fields change much more drastically over time than in the observations. This is consistent with the visual comparison of the fields and also with the differences in the estimates of z which as discussed below imply a faster temporal decorrelation in the predicted than the observed fields.

To understand the significance of the z value consider $L_2 = 2 \times L_1$ in the relationship $t_1/t_2 = (L_1/L_2)^z$. Then, for $z = 1$ (predictions) we get $t_2 = 2t_1$ and for $z = 1.4$ (observations) we get $t_2 = 2^{1.4} \times t_1 \simeq 3.4 \times t_1$. This implies that features twice as large will evolve two times slower in the predicted fields while they will evolve approximately 3.4 times slower in the observed fields. In other words, the predicted fields seem to have a faster decorrelation than the observed fields. It is interesting to compare the results of Figure 4.13 (and 4.5) with the schematic space-time diagram of hydrological processes in Figure 1.4 which shows a qualitatively very similar behaviour.

Another interesting comparison between the observed and predicted patterns resulted from comparison of their Depth–Area–Duration (DAD) curves for 1-hour duration. These curves plot depths of rainfall (here 1-hour accumulations) versus area of the storm over which these depths are equalled or exceeded. DAD curves compare the predicted and observed patterns in terms of their internal spatial structure irrespective of their locations. It was found that while the DAD curves tended to increase in the observed patterns from $t = 13$ to 15 hrs, they

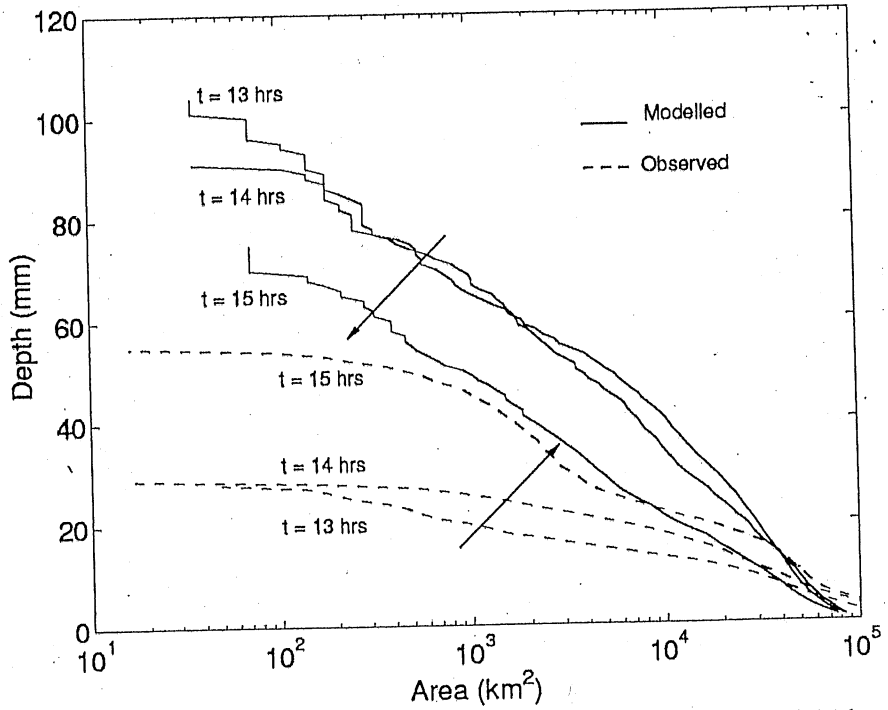

Figure 4.14. The solid lines show the DAD curves for $t = 13$, 14 and 15 hrs computed from the model-predicted 1-hour accumulation patterns; the broken lines show the same computed from the observed patterns.

tended to decrease in the predicted patterns (see Figure 4.14). Obviously, the tendency of the DAD curves to increase or decrease is related to the build-up or dissipation of the storm which might not be well reproduced in the model at least for the selected period of this particular storm. Such discrepancies would have significant effects on the predicted runoff and careful investigation and further study is warranted.

Overall, it was concluded that the above measures provided significant insight into subtle differences between the space-time structure of the predicted and observed patterns at a range of scales. These differences, although not fully interpreted yet, are much more informative than typical measures of forecast performance, such as threat scores and root-mean-square errors (see Wilks, 1995; or Fritsch et al., 1998). In addition, the scaling measures are normalised measures and are not influenced by how well the exact magnitudes and exact locations of rainfall intensities are predicted. Thus, they provide a direct assessment of how well the internal spatial structure and dynamics of the observed and predicted patterns compare to each other at a range of scales. It is hoped that these measures can provide useful feedback and guidance for improving numerical weather prediction models and this is an issue of current investigation.

4.6 CONCLUSIONS AND DISCUSSION

Many studies (for example, see Winchell et al., 1998 and references therein) have documented that the small-scale space-time variability of rainfall patterns has a

significant effect on the infiltration-excess runoff volume produced by a basin. Thus, severe underestimation of the basin runoff may result when the small-scale precipitation variability is ignored and a low-resolution precipitation input is supplied into a distributed rainfall-runoff model. Similarly, if the small-scale variability of rainfall is erroneously reproduced by an atmospheric model and these predictions are used for hydrologic studies, a severe impact on the predicted runoff hydrograph may result. Moreover, concerns about the effects of climate change on water resources at the basin scale require the ability to downscale the large-scale general circulation model (GCM) predictions and to reconstruct the small-scale space-time rainfall variability to be used as an input to a hydrologic model.

In this paper, a review of a class of current approaches in parameterising the space-time variability of rainfall patterns at a range of space-time scales was presented. Although we concentrated more on methodologies developed in our group, other approaches such as Over and Gupta (1996), Seed et al. (1999) and Marsan et al. (1996) could be used in a similar way. We favour approaches based on scale-invariance because their parameterisations are scale-independent (for example, parameters H and z in the schemes presented earlier). Such parameterisations are attractive because they are parsimonious and may be related to physical properties of the storm environment as compared with parameters which depend on scale.

It is reminded that if high-resolution precipitation patterns are available, H can be estimated directly from them via a multiscaling analysis. However, if only large-scale patterns are available and need to be downscaled, the parameter H needed in the downscaling scheme must be externally predicted or assumed. The same applies for the parameter z. As discussed, the variability in the parameter H has been found empirically to be well explained by the variability in the convective available potential energy (CAPE) of the prestorm environment (Perica and Foufoula-Georgiou, 1996a) and thus CAPE can be used to predict H. Prediction of the parameter z, which parameterises the space-time evolution of rainfall at a range of scales from a similar physical observable quantity, has not been studied yet. It is anticipated that z might be related to the temporal evolution of a vertical instability measure, for example, the change of CAPE over time ($\partial \mathrm{CAPE}/\partial t$) or to parameters describing parcel buoyancy and vertical wind shear (for example, see Weisman and Klemp, 1982). Empirical confirmation of the above assertions would require extensive meteorological observations not typically available (for instance, radiosonde observations are sparsely available in space and time). It could also well be that z can be empirically related to the standard deviation of $\Delta \ln I$ of the evolving fields. Although some preliminary evidence suggests such a possible relationship, a few cases deviated from this pattern. Analysis of more storms from different regions of the world and different climates must be done to provide an insight into the variability of the parameter z and its dependence on statistical or physical parameters of the atmosphere. Also, controlled experiments, via a state-of-the-art numerical weather prediction model which

can simulate precipitation fields together with other physically-consistent parameters of the atmosphere, might provide a way of overcoming the lack-of-dense-meteorological-observations gap and at least point to possible predictive relationships of z which can be further verified from observations.

Once the parameters H and z are available, we presented evidence that the space-time downscaling scheme developed by Venugopal et al. (1999b) is fairly successful in reproducing not only the spatial correlation of the rainfall fields at the subgrid scale, but also the temporal correlation. Preserving the temporal correlation might be important when the downscaled precipitation fields are to be used in a rainfall-runoff model or a coupled atmospheric-hydrologic model to predict soil-moisture fluxes and water and energy partitioning over a basin. This remains to be demonstrated via simulation studies.

For prediction of severe flood events several hours ahead of time, we rely on state-of-the-art three-dimensional non-hydrostatic storm prediction models which can predict rainfall patterns to be used in a hydrologic model. Although numerical weather prediction models have advanced impressively over the last decade, quantitative evaluation of their performance as far as their ability to accurately reproduce the space-time structure of precipitation patterns at a range of scales, lags behind. In this chapter, we have presented some recent efforts to develop new multiscale measures for quantitative precipitation forecast (QPF) assessment. Preliminary results suggest that numerical weather prediction models might not always perform well in capturing the space-time organisation structure of the observed rainfall fields and, in particular, they might have a tendency to produce patterns with less scale-to-scale spatial variability and faster temporal decorrelation. Analysis of more cases is needed to fully quantify discrepancies between the statistical structure of predicted and observed precipitation patterns and understand the sources (such as, physical parameterisations, data assimilation methods, model resolution etc.) of these discrepancies. The increased availability of high-resolution data from NEXRAD and increased computational resources available for such studies offer unique opportunities for scientific breakthroughs and advances in atmospheric/hydrologic research, quantitative precipitation forecasting, and flood forecasting over small to large-size basins.

ACKNOWLEDGEMENTS

The material presented in this paper draws upon the research of several past and current students. Special thanks are due to Jesus Zepeda-Arce whose M.S thesis formed the basis for the materials in Section 4.5. This research was supported over the years by NSF, NOAA and NASA. Specifically, we acknowledge the support of the joint GCIP-NOAA/NASA program (grant NAG8-1519), the NASA-TRMM Program Grant (NAG5-7715), a NASA Earth Systems Science Fellowship (NASA/NGTS-5014) to Venugopal Vuruputur, and a grant jointly supported by NSF and NOAA under the U.S. Weather Research Program (ATM-9714387). We also thank Robert Houze of the University of Washington

for providing us with the Darwin radar data, Jim Smith of Princeton University for providing us with the PRE-STORM data, and Kelvin Droegemeier of the University of Oklahoma for his collaboration on the storm-prediction research. Statistical analyses were performed at the Minnesota Supercomputer Institute, University of Minnesota.